Andreev resonances in the current-voltage characteristics of a normal-metal–superconductor junction

Santanu Chaudhuri and Philip F. Bagwell
School of Electrical Engineering, Purdue University, West Lafayette, Indiana 47907
(Received 20 December 1994; revised manuscript received 1 March 1995)

We calculate the current-voltage characteristic of a normal-metal–superconductor (NS) junction having a one-, two-, or three-dimensional electron emitter. An additional tunneling barrier is also placed in the junction, allowing the formation of quasibound Andreev energy levels. The resulting conductance resonances are strongest for a normal-metal–insulator–normal-metal–superconductor (NINS) junction, and are identical to the Rowell-McMillan oscillations in the three-dimensional case. Andreev resonances in the conductance of a NS junction generally become stronger when the electronic motion is confined to one dimension.

I. INTRODUCTION

The Bogoliubov-de Gennes (BdG) equations[1–3] describe the coupled motion of electrons and time-reversed electrons in a superconductor, a normal metal, and at their interfaces. The BdG equations can also describe conductance resonances due to combined Andreev and normal reflections in many different experimental geometries.[4–19] The most widely known of these conductance resonances are the Tomasch oscillations[5–7] in a normal-metal–superconductor–insulator–normal-metal (NSIN) geometry, and the Rowell-McMillan oscillations[8–11] in a normal-metal–insulator–normal-metal-superconductor (NINS) junction. In this paper we explore the effect of artificially confining electronic motion to a plane or a wire on conductance oscillations of both the Rowell-McMillan and Tomasch type.

Tomasch oscillations in a standard planar (three-dimensional) junction, can only be clearly observed in the differential conductance dI/dV or d^2I/dV^2, since they occur for voltages outside the superconducting energy gap where Andreev reflection is weak. Rowell-McMillan oscillations, on the other hand, also occur when the voltage is less than the superconducting energy gap; therefore, they can be directly observed in the I-V characteristic. Whenever the voltage exceeds the energy of an Andreev bound state trapped in the normal region between the superconductor and insulator, a corresponding step appears in the current of the NINS junction. Both the Tomasch and McMillan-Rowell oscillations are reviewed in Ref. 12.

The Tomasch type of conductance resonances become stronger when electronic motion is confined to one dimension. It may be possible to observe Tomasch oscillations directly in the I-V curve of a one dimensional conductor.[16] Unfortunately, these short-lived Andreev resonances in a NSIN (or NSIS) junction can still only be clearly observed in the differential conductance dI/dV or d^2I/dV^2 for a two- or three-dimensional junction. Strengthening the oscillations by restricting the geometry is not enough to overcome weakened Andreev reflection for energies outside the superconducting gap in a NSIS or NSIN junction.

Reference 16 also calculated the current-voltage characteristic of a one-dimensional Rowell-McMillan NINS layered geometry, using the method of Ref. 3, finding large Andreev resonances for applied voltages less than the superconducting gap. It was unclear from Ref. 16, however, why such an isolated Andreev resonance should still be observed after averaging over all the different possible directions from which electrons are injected in an ordinary three-dimensional planar tunneling junction. In ordinary resonant tunneling of normal electrons[20] for example, the strength of a similar type of oscillation is greatly reduced in a three-dimensional planar structure compared to an idealized one-dimensional structure.[21]

We show in this paper that strong Andreev resonances do indeed survive in a standard three-dimensional planar NINS junction, reducing there to the original Rowell-McMillan oscillations, and are only slightly weaker than for purely one-dimension electronic motion. This is because the transmission resonances for injection at an angle θ away from the tunnel barrier become very narrow at large θ, reducing dimensional broadening effects. It should be possible to study the reduced dimensional versions of Tomasch and Rowell-McMillan oscillations experimentally, using techniques similar to those currently employed in low-dimensional resonant tunneling.[22]

II. TRANSMISSION COEFFICIENTS

The BdG equations, describing the coupled motion of an electron u and its corresponding time-reversed electron v, are[1]

$$\begin{bmatrix} (H-\mu) & \Delta(r) \\ \Delta^*(r) & -(H-\mu) \end{bmatrix} \begin{bmatrix} u(r) \\ v(r) \end{bmatrix} = E \begin{bmatrix} u(r) \\ v(r) \end{bmatrix} . \quad (1)$$

The one-electron Hamiltonian H is

$$H = -\frac{\hbar^2}{2m}\left(\frac{\partial^2}{\partial x^2}+\frac{\partial^2}{\partial y^2}+\frac{\partial^2}{\partial z^2}\right)+V(x,y,z) . \quad (2)$$

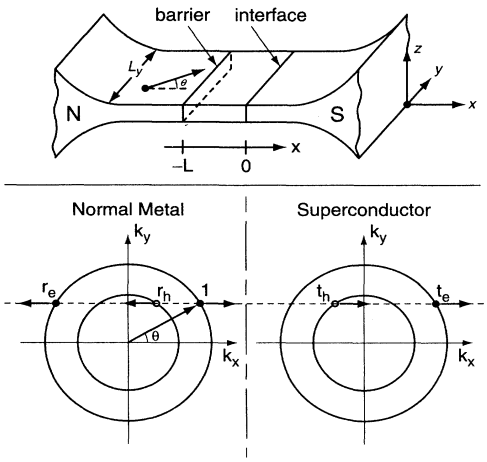

FIG. 1. Free electron motion parallel to the interface occurs in a two-dimensional NINS geometry. An electron from the normal metal is injected at an angle θ, producing the transmitted and reflected waves shown on the circles of constant energy. The wave vector k_y is conserved in the scattering process.

We restrict our attention to only sheet impurity scattering potentials of the form $V(x,y,z) = V_i\delta(x - x_i)$, since they can be engineered most easily in practice.

Figure 1(a) shows the geometry we consider in two dimensions, where the electron can be injected at any angle θ in the xy plane.[21] The solutions of Eq. (1) away from an interface have the form

$$\begin{bmatrix} u(x,y) \\ v(x,y) \end{bmatrix} = \begin{bmatrix} A \\ B \end{bmatrix} e^{ik_x x} e^{ik_y y} , \tag{3}$$

with the eigenvalues

$$E^2 = \left(\frac{\hbar^2 k_x^2}{2m} + \frac{\hbar^2 k_y^2}{2m} - \mu \right)^2 + \Delta^2 . \tag{4}$$

Due to translational invariance along the y direction, the wave vector k_y is a constant of the motion. The total energy E is also constant for each scattering state.

Figure 1(b) shows the constant energy surfaces far from the interfaces, in both the normal metal and superconductor. An electronlike quasiparticle incident from the normal-metal side scatters from the junction potential. To solve for the particle current transmission and reflection coefficients, we match $u(x,y)$, $v(x,y)$, and their derivatives at each boundary. Appendix A gives the details of this procedure. We make Andreev's approximation to describe scattering processes at the NS boundary; therefore, we neglect any normal reflections occurring at the NS boundary. In this approximation, normal reflections can occur only at the impurity.

We find the amplitude for Andreev reflection at the NS interface depends only on the total energy E, independent of the angle of incidence. Furthermore, the wave vector k_y is unchanged during the scattering process. Therefore, only the x component of the momentum k_x and the total energy E will determine the transmission and reflection coefficients. Hence all the results of Ref. 16 for the particle current reflection coefficients for both normal and Andreev processes will apply, with the total wave vector k replaced by its x component k_x. Similar conclusions hold for the corresponding three-dimensional scattering problem.

The electrical current can now be obtained in one dimension (1D) from[3]

$$I_{1D} = 2e \int_0^\infty \frac{dk_x}{2\pi} \frac{\hbar k_x}{m} \times [1 - R_e(E,k_x) + R_h(E,k_x)](f_N - f_S) , \tag{5}$$

in two dimensions (2D) using

$$I_{2D} = 2e \int_{-\infty}^\infty L_y \frac{dk_y}{2\pi} \int_0^\infty \frac{dk_x}{2\pi} \frac{\hbar k_x}{m} \times [1 - R_e(E,k_x) + R_h(E,k_x)](f_N - f_S) , \tag{6}$$

and in three dimensions (3D) by

$$I_{3D} = 2e \int_{-\infty}^\infty L_z \frac{dk_z}{2\pi} \int_{-\infty}^\infty L_y \frac{dk_y}{2\pi} \int_0^\infty \frac{dk_x}{2\pi} \frac{\hbar k_x}{m} \times [1 - R_e(E,k_x) + R_h(E,k_x)](f_N - f_S) . \tag{7}$$

Here $R_e(E,k_x)$ denotes the normal reflection probability and $R_h(E,k_x)$ the Andreev reflection probability. The Fermi factors are $f_N = f(E - eV)$ and $f_S = f(E)$. We convert Eqs. (5)–(7) to integrals over energy E and injection angle θ to do the actual current calculation, as described in the Appendix. In all figures we plot the normalized current I_N, defined as

$$I_{1D} = \frac{2e}{h} I_N^{1D} , \tag{8}$$

$$I_{2D} = \frac{2e}{h} \frac{L_y k_F}{\pi} I_N^{2D} , \tag{9}$$

and

$$I_{3D} = \frac{2e}{h} \frac{L_y L_z k_F^2}{4\pi} I_N^{3D} . \tag{10}$$

The normalization factors are chosen so that I_N for a ballistic NS interface is the same function of voltage in 1D, 2D, and 3D.

III. CURRENT-VOLTAGE CHARACTERISTICS

In the following calculations we assume the Fermi energy μ =1 eV and the order parameter $|\Delta|$ = 10 meV, typical for metals. The choices fix the Fermi wavelength as λ = 12.3 Å and the coherence length as ξ_0 = 196 Å, assuming m is the free electron mass. For the tunneling barrier, we assume the transmission coefficient $T \simeq 0.2$. In the normal state we have[3] $T = 1/(1 + Z^2)$, so that the parameter $Z = 2.0$ for an electron normally incident on the tunnel barrier at the Fermi velocity. Our results do not strongly qualitatively depend on these parameter

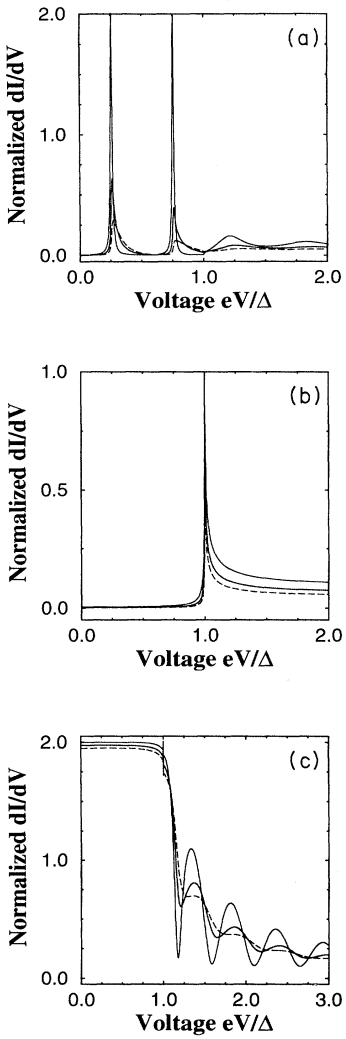

FIG. 2. Normalized differential conductance dI/dV vs bias voltage V when the impurity is (a) 1000 Å inside the normal metal, (b) at the NS interface, and (c) 1000 Å inside the superconductor. The device geometry permits either one-dimensional (solid), two-dimensional (dotted), or three-dimensional (dashed) electronic motion.

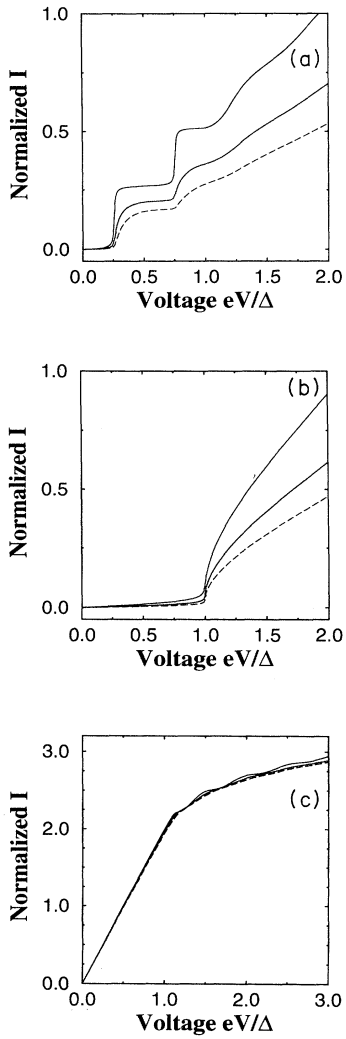

FIG. 3. Normalized current I vs bias voltage V when the impurity is (a) 1000 Å inside the normal metal, (b) at the NS interface, and (c) 1000 Å inside the superconductor. The device geometry permits either one-dimensional (solid), two-dimensional (dotted), or three-dimensional (dashed) electronic motion.

choices, provided the tunnel barrier is not too transmissive.

Figure 2 shows the differential conductance dI/dV versus voltage V of the NS junction when the tunnel barrier is (a) embedded in the normal-metal 1000 Å from the NS interface, (b) at the NS interface, and (c) embedded in the superconductor 1000 Å from the NS interface. This corresponds to (a) a NINS McMillan-Rowell junction, (b) a NIS Giaever tunneling junction, and (c) a NSIS Tomasch-type geometry. Figures 3(a)–(c) shows the corresponding current versus voltage obtained by integrating Figs. 2(a)–(c), respectively. The resonances in dI/dV from Figs. 2(a) and (c) generally become broader, weaker, and shift to higher voltages as the injected electron distribution changes from 1D to 2D and 3D. Conversely, the Giaever tunneling result in Fig. 2(b) is relatively immune to altering the spatial distribution of injected electrons.

The strongest resonant oscillations in dI/dV occur in Fig. 2(a), and are surprisingly resistant to averaging over the angular distribution of the injected electrons. To qualitatively understand Fig. 2(a), note that the momentum along the tunneling direction decreases with angle as $\hbar k_x = \sqrt{2mE}\cos\theta$. A larger total energy E is now required to meet the resonance condition for k_x, shifting the resonance at an angle θ to a higher energy. This contributes to broadening of the conductance resonances in dI/dV. However, because of the smaller momentum $\hbar k_x$ along the x direction, the tunnel barrier looks effectively much more reflecting for injection at an angle θ. The transmission parameter $Z = V_i/\hbar v_x$ for transmission at an angle θ, so the resonances in $[1 - R_e(E,\theta) + R_h(E,\theta)]$ versus energy E are much narrower for $\theta \neq 0$ than at normal incidence.

The narrowing of the resonances in $[1 - R_e(E,\theta) +$

$R_h(E,\theta)$] at large injection angles greatly reduces the dimensional broadening of resonances in the differential resistance dI/dV. Corresponding Andreev resonances can be observed in Fig. 2(a) in 1D, 2D, and 3D. The 3D oscillations in Fig. 2(a) are simply the derivative of the Rowell-McMillan oscillations, and produce relatively clear current steps in the I-V in Fig. 3(a). Even for the 3D junction, the single current step near eV = 0.75 Δ is clearly visible. Increasing the distance L of the tunnel barrier from the NS interface will produce more such current steps.[10] This same mechanism narrowing the transmission resonances at an angle θ also explains why the Giaever tunneling current in Fig. 2(b) becomes more sharply peaked in 3D than in 2D or 1D. Averaging the electron injection over all angles does not appreciably broaden the onset of Giaever tunneling.

The weak oscillations occurring above the superconducting gap in Fig. 2(c) and Fig. 3(c) for this NSIS junction strongly resemble the Tomasch oscillations in a NSIN geometry. In the NSIN Tomasch geometry, an electron incident on the insulator from the superconductor can either Andreev reflect or normally reflect. The fraction of electrons Andreev reflecting can be viewed as conducting through an effective NSN geometry, while those normally reflecting can be viewed as moving in an effective NSIS geometry. If the insulating barrier is strong, conduction through the NSIN geometry is nearly equivalent to conducting through a NSIS geometry. If the insulator is only moderately strong, the standard NSIN Tomasch geometry will therefore produce a more complicated interplay of resonances than the simplified NSIS geometry considered here. The resonances in any of these Tomasch-type geometries will be equally difficult to observe directly in the I-V characteristic of a junction. Figure 3(c) implies this observation might barely be possible for a 1D NSIS junction.

In Figs. 2(c) and 3(c), the impurity is several coherence lengths inside the superconductor ($L > \xi_0$), so that few quasiparticles reach the barrier for eV $< \Delta$. The junction therefore appears nearly ballistic for eV $< \Delta$, producing similar normalized currents for 1D, 2D, and 3D tunneling junctions. We show in the Appendix that the normalized currents are in fact equal for a ballistic NS junction, and Fig. 3(c) nearly approximates such a junction.

Isolated Andreev resonances of the Rowell-McMillan type in low-dimensional structures may also already have been observed by tunneling from a scanning tunneling microscope tip into a small metallic island on a superconducting substrate.[11] However, disordered interfaces may have clouded their observation in Ref. 11. Andreev resonances in a planar (three-dimensional) NINIS geometry may also explain the zero bias conductance peak seen in Ref. 18, since averaging over a distribution of such resonances produces a similar conductance peak in a one-dimensional model.[19]

IV. CONCLUSIONS

Both the Rowell-McMillan and Tomasch-type oscillations in the I-V characteristic of NINS and NSIS junctions, respectively, are analogous to the quasibound states in a resonant tunneling diode (NININ junction). In the NINS junction, the resonant energy levels are formed by multiple Andreev reflections from the NS junction and normal reflections from the tunnel barrier, instead of the multiple reflections between two tunnel barriers in the NININ junction. Just as for the resonant tunneling diode, the resonant energy levels in the NINS junction are directly observable in its current-voltage characteristic.[8]

It should be possible to carry out a low-dimensional version of the Rowell-McMillan and Tomasch experiments. A semiconductor-based NINS junction suitable for observing isolated Andreev resonances can be formed by placing superconducting contact metallization on a molecular beam epitaxially grown GaAs-$Al_xGa_{1-x}As$-GaAs or InAs-AlSb-InAs heterostructure. This structure could then be etched into a quasi-one-dimensional wire or post, using techniques similar to those used to fabricate low-dimensional resonant tunnel junctions for normal electrons.[22] In this paper we have shown that resonances in the differential conductance dI/dV should become more clearly observable in a low-dimensional version of either the Rowell-McMillan or Tomasch experiment.

APPENDIX: SCATTERING FROM THE NINS POTENTIAL

We take the x direction to be normal to the interfaces, as in Fig. 1(a). The wave vectors for motion in the x direction at an energy E are then

$$k_{\pm}^{x} = \sqrt{\frac{2m}{\hbar^2}(\mu + E)}\ \cos\theta \tag{A1}$$

in the normal metal and

$$q_{\pm}^{x} = \sqrt{\frac{2m}{\hbar^2}(\mu + \sqrt{E^2 - \Delta^2})}\ \cos\theta_s \tag{A2}$$

in the superconductor. Here θ is the angle of the wave vector k incident from the normal metal to the x axis, and θ_s the angle of the wave vector q inside the superconductor. We determine θ_s from

$$\frac{\sin^2\theta_s}{\sin^2\theta} = \frac{\mu + E}{\mu + \sqrt{E^2 - \Delta^2}}\ . \tag{A3}$$

We make Andreev's approximation to neglect differences between the wave vectors k and q when $\Delta \ll \mu$, unless they occur in an exponent. Furthermore, we neglect the small difference between θ and θ_s, even in an exponent. These approximations do not qualitatively change any of the results for the conductance.

To obtain the normal and Andreev reflection coefficients for electron injection from the normal metal, we replace the total wave vectors in Ref. 16 with their x components. The electron and hole particle current reflection amplitudes when the impurity is located in the normal metal are therefore[16]

$$r_e = \frac{1}{d}\left(\frac{-iZ}{1+iZ}\right)\left[1-\left(\frac{v_0}{u_0}\right)^2 e^{2i(k_+^x-k_-^x)L}\right], \quad \text{(A4)}$$

and

$$r_h = \frac{1}{d}\left(\frac{v_0}{u_0}\right)\left(\frac{1}{1+Z^2}\right) e^{-i\phi} e^{i(k_+^x-k_-^x)L}. \quad \text{(A5)}$$

The resonant denominator d in Eqs. (A4) and (A5) is given by

$$d = 1-\left(\frac{Z^2}{1+Z^2}\right)\left(\frac{v_0}{u_0}\right)^2 e^{2i(k_+^x-k_-^x)L}. \quad \text{(A6)}$$

Here L is the distance of the impurity from the NS interface, Z is the normalized impurity strength given by $Z = V_i/\hbar v_x$, and ϕ is the phase of the superconducting order parameter. The coherence factors u_0 and v_0 are found from

$$2u_0^2 = 1+\frac{\sqrt{E^2-\Delta^2}}{E} \quad \text{(A7)}$$

and

$$2v_0^2 = 1-\frac{\sqrt{E^2-\Delta^2}}{E}. \quad \text{(A8)}$$

Similarly, if the impurity is a distance L inside the superconductor, the transmission and reflection amplitudes become

$$r_e = \frac{1}{d}\left(\frac{-iZ}{1+iZ}\right)\left[1-\left(\frac{v_0}{u_0}\right)^2\right] e^{2iq_+^x L} \quad \text{(A9)}$$

and

$$r_h = \frac{1}{d}\left(\frac{v_0}{u_0}\right)\left[1-\left(\frac{Z^2}{1+Z^2}\right) e^{2i(q_+^x-q_-^x)L}\right] e^{-i\phi}. \quad \text{(A10)}$$

In this case, we find d in Eqs. (A9) and (A10) from

$$d = 1-\left(\frac{Z^2}{1+Z^2}\right)\left(\frac{v_0}{u_0}\right)^2 e^{2i(q_+^x-q_-^x)L}. \quad \text{(A11)}$$

Equations (A4)–(A6) and (A9)–(A11) hold when the energy satisfies $E > 0$. Similar formula can be obtained for $E < 0$.

The resonant energy levels are obtained by setting $d = 0$ in either Eqs. (A6) or (A11). Note that these oscillations are of the "4d" type,[12] where both the electron and the hole must each traverse the resonant cavity twice to form a bound state. Various nonideal effects,[12] which we neglect in this paper, could contribute a small "2d" component to the oscillation period.

Equations (A4) and (A5) and (A9) and (A10) show that, for a ballistic NS interface, the particle current reflection amplitudes for normal and Andreev reflection are independent of the incident angle. The reflection amplitudes then depend only on the total energy of the incident particle, the same as in a one-dimensional NS junction. The reflection probabilities are $R_e = |r_e|^2$ for normal reflection and $R_h = |r_h|^2$ for Andreev reflections.

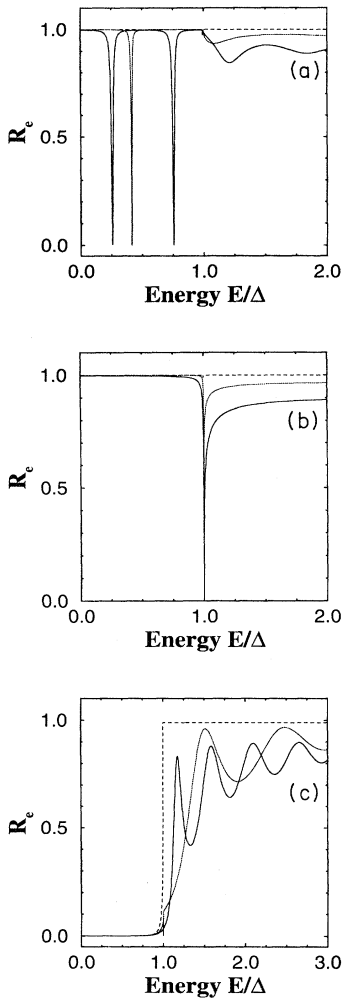

FIG. 4. Normal reflection coefficient R_e as a function of the incident energy E when the impurity is (a) 1000 Å inside the normal metal, (b) at the NS interface, and (c) 1000 Å inside the superconductor. The angle of incidence is $\theta = 0$ (solid), $\theta = 57°$ (dotted), and $\theta = 89°$ (dashed).

We can understand the resistance of dI/dV to angular averaging in Fig. 2(a) by examining the normal reflection R_e from Fig. 4(a) and Andreev reflection R_h from Fig. 5(a). As the injection angle θ increases, the resonance shifts to higher energy, becomes narrower, and may disappear altogether. All formula for resonance energies and linewidths from Ref. 16 hold also for injection at an angle θ, provided we replace the physical length L by the "effective length" $L\cos\theta$ and the total velocity v by its x component v_x. The total resonant energy E_R therefore increases to approximately by $E_R \simeq \pi\Delta\xi_0 n/2L\cos\theta$, shifting the resonances in dI/dV to a higher voltage and broadening them. Conversely, the resonance width E_I is approximately $E_I \simeq -\ln(RR_a)\Delta\xi_0/2L\cos\theta$. The Andreev reflection coefficient of a ballistic NS junction is $R_a \simeq 1$ for $E_R < \Delta$. The reflection coefficient in the

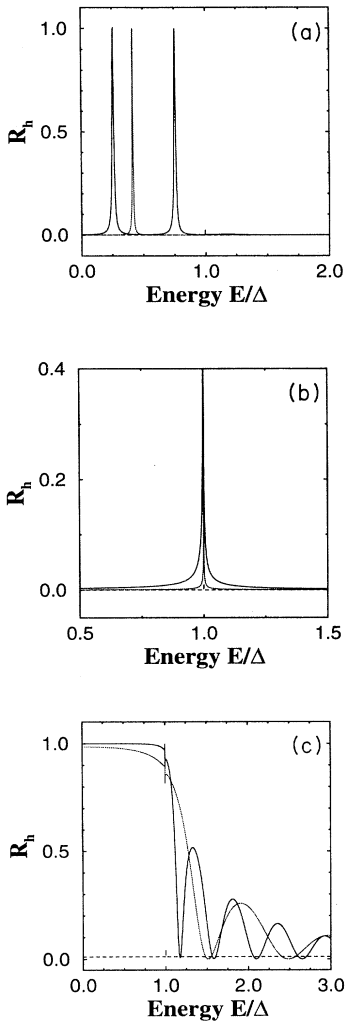

FIG. 5. Andreev reflection coefficient R_h as a function of the incident energy E when the impurity is (a) 1000 Å inside the normal metal, (b) at the NS interface, and (c) 1000 Å inside the superconductor. The angle of incidence is $\theta = 0$ (solid), $\theta = 57°$ (dotted), and $\theta = 89°$ (dashed).

absence of superconductivity is $R = Z^2/1 + Z^2$, with $Z = V_i/\hbar v_x = V_i/\cos\theta\sqrt{2E/m}$. Therefore, as the injection angle approaches $\theta \to \pi/2$ we have $R \to 1$, independent of the initial barrier strength V_i. This narrows the transmission resonances considerably for large angles.

Similar reasoning applies to the reflection coefficients for the tunnel junction in Figs. 4(b) and 5(b). As is evident from Fig. 4(b), electron reflection is only $R_e \simeq 0.9$ when $E = 2\Delta$ and $\theta = 0$. The reflection increases considerably at large angles, since the barrier appears effectively stronger. The corresponding dI/dV in Fig. 2(b) is therefore sharpest in 3D, where more large angle electrons are injected from the contacts.

At large injection angles, the resonances are also pushed to higher energy in Figs. 4(c) and 5(c), when the impurity is in the superconductor. The effective normal reflection R from the barrier also increases, as before. However, the Andreev reflection R_a decreases drastically as the resonance energy increases, since the resonance energy is now outside the superconducting energy gap ($E_R > \Delta$). Consequently, the resonances are pushed to higher energy and broadened when the impurity is in the superconductor. That is why the resonances in dI/dV are so poorly resolved in 3D in Fig. 2(c), compared to their good resolution in 3D in Fig. 2(a). Formulas similar to those used in Ref. 16 describe the evolution of these resonances in Figs. 4(c) and 5(c).

We now wish to obtain the electrical current from the reflection coefficients in Eqs. (A4) and (A5) and (A9) and (A10). To facilitate our evaluation of Eqs. (5)–(7), we convert the integrals over the x, y, and z components of the wave vector to an integration over total energy E and angle of incidence θ. The total energy in the normal metal can be written as

$$E^2 = \left(\frac{\hbar^2 k_r^2}{2m} - \mu\right)^2 , \tag{A12}$$

where the radial wave vector is $k_r^2 = k_x^2 + k_y^2$ in two dimensions and $k_r^2 = k_x^2 + k_y^2 + k_z^2$ in three dimensions. We transform further to to polar coordinates using $dk_x dk_y = k_r dk_r d\theta$ in two dimensions and $dk_x dk_y dk_z = k_r^2 \sin\theta dk_r d\theta d\phi$ in three dimensions. Using $k_x = k_r \cos\theta$ and $dE/h = \hbar k_r dk_r/2\pi m$, we obtain the normalized currents

$$I_N^{1D} = \int_{-\infty}^{\infty} dE \times[1 - R_e(E,\theta=0) + R_h(E,\theta=0)](f_N - f_S) \tag{A13}$$

in one dimension,

$$I_N^{2D} = \frac{1}{2}\int_{-\pi/2}^{\pi/2} d\theta \cos\theta \int_{-\infty}^{\infty} dE \sqrt{1 + \frac{E}{\mu}} \times[1 - R_e(E,\theta) + R_h(E,\theta)](f_N - f_S) \tag{A14}$$

in two dimensions, and

$$I_N^{3D} = 2\int_0^{\pi/2} d\theta \sin\theta\cos\theta \int_{-\infty}^{\infty} dE \left(1 + \frac{E}{\mu}\right) \times[1 - R_e(E,\theta) + R_h(E,\theta)](f_N - f_S) \tag{A15}$$

in three dimensions.

The differential conductance dI/dV at $T = 0$ can be found from Eqs. (A13)–(A15). At zero temperature we have

$$\frac{d}{dV}(f_N - f_S) = -\left.\frac{df}{dE}\right|_{E=eV} = \delta(E - eV) . \tag{A16}$$

The normalized differential conductance is then found from the angular integrations

$$\left(\frac{dI_N}{dV}\right)_{1D} = [1 - R_e(E = eV, \theta = 0) + R_h(E = eV, \theta = 0)] \tag{A17}$$

in one dimension,

$$\left(\frac{dI_N}{dV}\right)_{2D} = \frac{1}{2}\int_{-\pi/2}^{\pi/2} d\theta \cos\theta \,[1 - R_e(E = eV, \theta) + R_h(E = eV, \theta)] \quad \text{(A18)}$$

in two dimensions, and

$$\left(\frac{dI_N}{dV}\right)_{3D} = 2\int_{0}^{\pi/2} d\theta \sin\theta \cos\theta [1 - R_e(E = eV, \theta) + R_h(E = eV, \theta)] \quad \text{(A19)}$$

in three dimensions.

[1] P.G. de Gennes, *Superconductivity of Metals and Alloys* (Addison-Wesley, New York, 1989).
[2] W.N. Mathews, Jr., Phys. Status Solidi B **90**, 327 (1978).
[3] G.E. Blonder, M. Tinkham, and T.M. Klapwijk, Phys. Rev. B **25**, 4515 (1982).
[4] P.G. de Gennes and D. Saint-James, Phys. Lett. **4**, 151 (1963).
[5] W.J. Tomasch, in *Tunneling Phenomena in Solids*, edited by E. Burstein and S. Lundqvist (Plenum, New York, 1969).
[6] T. Wolfram, Phys. Rev. **170**, 481 (1968).
[7] J. Demers and A. Griffin, Can. J. Phys. **49**, 285 (1971).
[8] J.M. Rowell, Phys. Rev. Lett. **30**, 167 (1973).
[9] L. Wong, S. Shih, and W.J. Tomasch, Phys. Rev. B **23**, 5775 (1981).
[10] G.B. Arnold, J. Low Temp. Phys. **59**, 142 (1985). See Fig. 4. Making the normal region longer in this calculation would reproduce the multiple Rowell-McMillan current steps.
[11] S.H. Tessmer, D.J. van Harlingen, and J.W. Lyding, Phys. Rev. Lett. **70**, 3135 (1993).
[12] E.L. Wolf, *Principles of Electron Tunneling Spectroscopy* (Oxford, New York, 1985).
[13] A. Hahn, Phys. Rev. B **31**, 2816 (1985).
[14] F. Stageberg, R. Cantor, A.M. Goldman, and G.B. Arnold, Phys. Rev. B **32**, 3292 (1985); M.J. DeWeert and G.B. Arnold, Phys. Rev. Lett. **55**, 1522 (1985); Phys. Rev. B **39**, 11 307 (1989).
[15] P.C. van Son, H. van Kempen, and P. Wyder, Phys. Rev. B **37**, 5015 (1988).
[16] R.A. Riedel and P.F. Bagwell, Phys. Rev. B **48**, 15 198 (1993); P.F. Bagwell, R.A. Riedel, and L. Chang, Physica B **203**, 475 (1994).
[17] M.J.M. de Jong and C.W.J. Beenakker (unpublished).
[18] B.J. van Wees, P. de Vries, P. Magnee, and T.M. Klapwijk, Phys. Rev. Lett. **69**, 510 (1992).
[19] V.A. Khlus, A.V. Dyomin, and A.L. Zazunov, Physica C **214**, 413 (1993); V.A. Khlus and A.V. Dyomin (unpublished).
[20] T.P.E. Broekaert, W. Lee, and C.G. Fonstad, Appl. Phys. Lett. **53**, 1545 (1988).
[21] P.F. Bagwell, T.P.E. Broekaert, and T.P. Orlando, J. Appl. Phys. **68**, 4634 (1990).
[22] M.A. Reed, J.N. Randall, R.J. Aggarwal, R.J. Matyi, T.M. Moore, and A.E. Wetsel, Phys. Rev. Lett. **60**, 535 (1988).